
Symbol-LLM: Leverage Language Models for Symbolic System in Visual Human Activity Reasoning

Xiaoqian Wu Yong-Lu Li* Jianhua Sun Cewu Lu*
Shanghai Jiao Tong University
{enlighten, yonglu_li, gothic, lucewu}@sjtu.edu.cn

Abstract

Human reasoning can be understood as a cooperation between the intuitive, associative “System-1” and the deliberative, logical “System-2”. For existing System-1-like methods in visual activity understanding, it is crucial to integrate System-2 processing to improve explainability, generalization, and data efficiency. One possible path of activity reasoning is building a symbolic system composed of symbols and rules, where one rule connects multiple symbols, implying human knowledge and reasoning abilities. Previous methods have made progress, but are defective with limited symbols from handcraft and limited rules from visual-based annotations, failing to cover the complex patterns of activities and lacking compositional generalization. To overcome the defects, we propose a new symbolic system with two ideal important properties: broad-coverage symbols and rational rules. Collecting massive human knowledge via manual annotations is expensive to instantiate this symbolic system. Instead, we leverage the recent advancement of LLMs (Large Language Models) as an approximation of the two ideal properties, *i.e.*, Symbols from Large Language Models (**Symbol-LLM**). Then, given an image, visual contents from the images are extracted and checked as symbols and activity semantics are reasoned out based on rules via fuzzy logic calculation. Our method shows superiority in extensive activity understanding tasks. Code and data are available at https://mvig-rhos.com/symbol_llm.

1 Introduction

Human reasoning can be understood as a cooperation between two cognitive systems: the intuitive, associative “System-1” and the deliberative, logical “System-2” [36]. An example of System-2 reasoning is illustrated in Fig. 1a. A feather and an iron ball are dropped at the same height in a vacuum, which one will land first? Human intelligence derives the answer from the Universal Gravitation Law, *i.e.*, reasoning in a physical symbolic system to avoid intuitive errors. As a critical component in building AI systems, visual activity understanding urgently needs System-2 reasoning. Previous works [37, 21, 41, 24] typically establish the mapping between visual inputs and natural language, where knowledge is embedded into some non-symbolic form such as the weights of language models [35]. Though effective, these System-1-like methods depend on large-scale visual data, thus suffering from diminishing marginal utility. Also, it fails in explainability and generalization due to black-box computing. Thus, it is important to integrate System-2 reasoning.

With one glance at an image, we can effortlessly ground visual inputs to symbols/concepts and apply commonsense reasoning to imagine the world beyond the pixels, a process similar to the gravity case. Fig. 1b shows a possible path for System-2 visual reasoning for human activity: a symbolic system composed of symbols and rules. One rule “Hip seated in a boat \wedge Hands control an engine \wedge Hands hold onto the side of a boat \models Human ride a boat” connects symbols

*Corresponding authors.

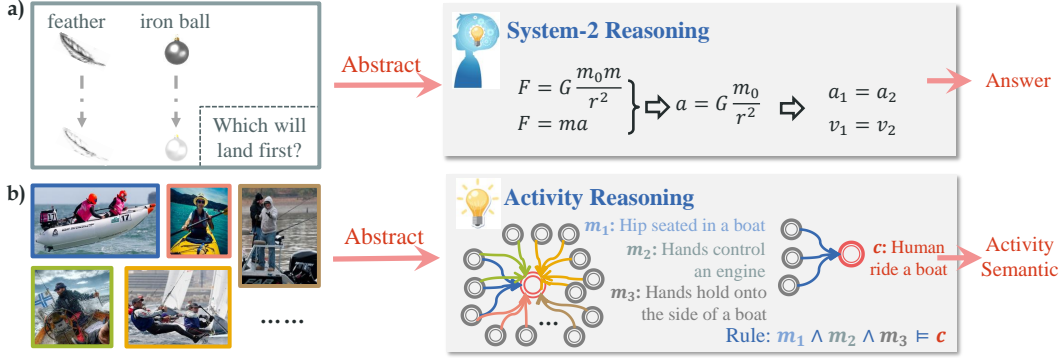


Figure 1: System-2 reasoning in a) solving physical questions and b) understanding human activities. They both involve a symbolic system implying human commonsense.

(e.g., “Hands control an engine” “Human ride a boat”) and implies human commonsense. Then, given an image, symbols are first extracted from visual inputs and then activity semantics are deduced based on rules. In this paper, we focus on this line of System-2 reasoning and zoom in from general visual understanding to human activities in various complex contexts, which is a challenging problem in visual understanding.

Current activity reasoning methods are not well equipped with System-2 reasoning. For instance, HAKE [28, 26] adopts a similar path as Fig. 1b from the perspective of human body part states and makes progress toward activity reasoning, but is defective with *limited symbols from handcraft* (93 primitives) and *limited rules* from visual-based annotations (100 K+ images). For example, Fig. 1b shows several rules related to the activity “Human ride a boat”, e.g.,

- (R1, green) Hip seated in a boat \wedge Hand hold onto the side of the boat \wedge Hand operate the steering wheel \models Human ride a boat
- (R2, orange) A rope is attached to a boat \wedge Hand hold the rope \wedge Hand adjust a sail \wedge Feet hold onto the rope \wedge Leg stretched out \models Human ride a boat

However, the rules summarized by [26] are “(R3) Hip sit in \wedge Hand hold \models Human ride a boat” “(R4) Hand hold \wedge Feet close with \models Human ride a boat”, which fail to cover the complex patterns of human activities. Thus, it lacks compositional generalization, i.e., a generalized understanding of visual concepts, their relationships, and their novel combinations.

In view of this problem, we propose a novel symbolic system that implies abundant human knowledge and organizes diverse reasonable rules as in Fig. 1b. To achieve this, the symbols should be with **broad semantic coverage** to express various activity contexts. Moreover, the rules should be **rational and unambiguous**. R4 is a failure case, where ‘Hand hold’ and ‘Feet close with’ do not necessarily lead to “Human ride a boat”, and “Human tie a boat” “Human exit a boat” are other possible conclusions. Ambiguous semantics should be corrected in rules to avoid confusion. Collecting massive human knowledge via manual annotation is expensive to instantiate this symbolic system. Our main insight is Symbols from Large Language Models (**Symbol-LLM**), i.e., leveraging the recent advancement of Large Language Models (LLMs) to approximate the above two important properties. This is achieved by the *symbol-rule loop* and *entailment check* strategy. Then, the symbolic system can be used to reason with visual inputs, where visual contents from the images are *extracted and checked* as symbols and activity semantics are reasoned out via *fuzzy logic calculation*.

In conclusion, our main contributions are: **1)** We point out that current System-2 reasoning [26] suffers from a defective symbolic system with hand-crafted symbols and limited, ambiguous rules. **2)** To overcome the defects, we propose a novel symbolic system with broad-coverage symbols and rational rules. Further, we propose Symbol-LLM to instantiate it and show how it helps visual reasoning. **3)** In extensive activity understanding tasks, our method shows superiority in explainability, generalization, and data efficiency.

2 Related Work

Activity Understanding [29, 12] is still a difficult task compared with object detection [39] or pose estimation [11]. This is caused by its complex visual patterns and long-tail data distribution [43].

There are mainly image-based [5, 19], video-based [18, 4] and skeleton-based [42, 8] methods. In this paper, we focus on image-based methods.

Vision-Language Models (VLMs) have been intensively studied recently. Trained with web-scale image-text pairs, they can make zero-shot predictions on various recognition tasks [48] including human activities. Though effective, previous System-1-like methods [37, 21, 41, 24] need to be improved in explainability, generalization, and data efficiency. Thus, integrating System-2 reasoning, which is our main focus, is important.

Probabilistic Programming [38, 13] unifies probabilistic modeling and traditional programming. We follow the principles of the standard first-order logic (FoL) in probabilistic programming, *e.g.*, logical connectives \wedge, \vee . The standard FoL typically solves simplified relational tasks, where symbols are definitely True/False. However, when adapting FoL in vision reasoning tasks, the symbols are not known to be True/False. Instead, the models are required to predict the symbol probabilities (usually via a neural network). Thus, a hybrid “neuro-symbolic” method is adopted.

Neuro-Symbolic Reasoning provides a possible way of combining System-1 and System-2 learning, where knowledge is represented in symbolic form and learning and reasoning are computed by a neural network. [15]. Recently, researchers utilize neural-symbolic reasoning in tasks including visual question answering [2, 20, 45, 35, 40], decision-making [7], motion programming [23], scene understanding [31]. Focused on activity reasoning, HAKE [28, 26] propose an intermediate space spanned by human body part states as primitives. To overcome its inherent defect in compositional generalization, we propose a novel symbolic system with broad semantics and rational rules.

3 Method

3.1 Formulating the Symbolic System

3.1.1 Structure

We first analyze the structure of the symbolic system. As aforementioned, the activity symbolic system is composed of rules that connect symbols, which implies human knowledge and reasoning abilities. Formally, one rule involves several symbols, where one of them is the *conclusion* and the others are *premises*. Each rule takes the form $r : m_1 \wedge m_2 \wedge \dots \wedge m_{n_r} \models c$, where $M = \{m_i\}_{i=1}^{n_r}$ is the premise set and c is the conclusion. Each conclusion corresponds to more than one rule with varied combinations of premise symbols because one activity typically has different visual patterns. Multiple rules for one conclusion are logically connected with \vee , *i.e.*, one conclusion holds if at least one rule is satisfied. A hyper-graph is a proper data structure to handle the complexity of the connection. Therefore, we define the structure of the activity symbolic system as a \mathcal{B} -Graph [14].

Definition 1. (Directed Hypergraph [3]) A hypergraph is a generalization of a graph in which an edge can join any number of vertices. A directed hypergraph is a pair $(\mathcal{X}, \mathcal{E})$, where \mathcal{X} is a set of vertices, and \mathcal{E} is a set of pairs of subsets of \mathcal{X} . Each of these pairs $(D, C) \in \mathcal{E}$ is a hyperedge; the vertex subset D is its domain, and C is its codomain.

Definition 2. (\mathcal{B} -Graph [14]) A \mathcal{B} -graph is a type of directed hypergraph with only \mathcal{B} -arcs. A \mathcal{B} -arch is a type of a hyperedge that is directed to a single head vertex, and away from all its other vertices.

Definition 3. (Activity Symbolic System) The activity symbolic system $(\mathcal{S}, \mathcal{R})$ is a \mathcal{B} -Graph, where \mathcal{S} is a set of vertices/symbols, and \mathcal{R} is a set of pairs of subsets of \mathcal{S} . Each of these pairs $r = (M, C) \in \mathcal{R}$ is a hyperedge/rule; the vertex subset $M = \{m_i\}_{i=1}^{n_r}$ is its domain/premises, and $C = \{c\}$ is its codomain/conclusion. Equivalently, a rule takes the form $r : \bigwedge_{m \in M} m \models c$. Since $|C| = 1$, r is a \mathcal{B} -arch.

Definition 4. (Decomposition of Activity Symbolic System) One conclusion c^* corresponds to one symbolic sub-system $(\mathcal{S}_{c^*}, \mathcal{R}_{c^*})$, where $\mathcal{S}_{c^*} \subseteq \mathcal{S}$, $\mathcal{R}_{c^*} \subseteq \mathcal{R}$. $\forall r = (M, C) \in \mathcal{R}_{c^*}$, $C = \{c^*\}$. $\forall s \in \mathcal{S}_{c^*} \setminus \{c^*\}$, $\exists r = (M, C) \in \mathcal{R}_{c^*}$, $s \in M$.

Def. 3,4 is depicted in Fig. 2. Def. 3 is based on Def. 1,2 and analysis above. In applications, we typically judge a specific conclusion with other symbols/rules removed. It is achieved by decomposing the activity symbolic system (graph) into sub-systems (sub-graphs) in Def. 4.

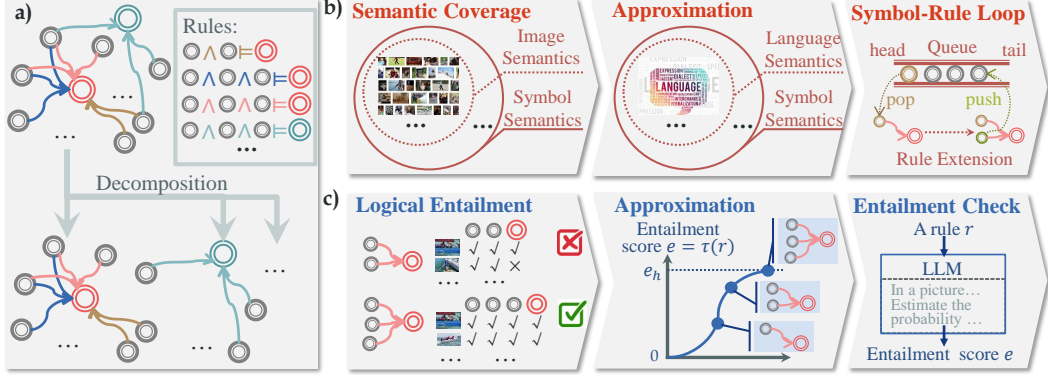


Figure 2: Our activity symbolic system. **a)** Structure and decomposition of the symbolic system (Sec. 3.1.1). **b)** Semantic coverage (Sec. 3.1.2). It can be approximated based on LLMs’ knowledge and achieved via the symbol-rule loop (Sec. 3.2.1). **c)** Logical entailment (Sec. 3.1.2). It can be approximated based on an entailment scoring function and achieved by entailment check (Sec. 3.2.2).

3.1.2 Two Ideal Properties

Existing methods [28, 26] can also be formulated under this structure. However, they fail to cover the complex patterns of activities and lack compositional generalization. To overcome the defects, we propose two important ideal properties: 1) symbols should be with broad *semantic coverage* to express different conditions in the activity image database; 2) rules should satisfy *logical entailment* [9] to add rationality and avoid ambiguity, *i.e.*, the premises set should lead to the conclusion without exception. They are formulated in Def. 5,6 and illustrated in Fig. 2b,c.

Definition 5. (Semantic Coverage of Activity Symbolic System) Given a very large-scale activity images database $\mathcal{D} = \{(I, A_I, \mathcal{S}_I)\}$ (I : image, A_I : ground-truth activities happening in I , \mathcal{S}_I : ground-truth symbols happening in I), then $\forall (I, A_I, \mathcal{S}_I) \in \mathcal{D}, \forall s \in \mathcal{S}_I, s \in \mathcal{S}$.

Definition 6. (Logical Entailment of Activity Symbolic System) $\forall r = (M, C) \in \mathcal{R}, M = \{m_i\}_{i=1}^{n_r}$, we have:

1. $\forall (I, A_I, \mathcal{S}_I) \in \mathcal{D}$, if $M \subset \mathcal{S}_I$, then $c \in A_I$;
2. $\forall 1 \leq i \leq n_r, \exists (I, A_I, \mathcal{S}_I) \in \mathcal{D}, M \setminus \{m_i\} \subset \mathcal{S}_I$, but $c \notin A_I$.

3.2 Instantiating the Symbolic System

To instantiate the proposed symbolic system, it is expensive to collect massive human knowledge via manual annotation as in HAKE [28, 26]. Instead, we use LLMs which have profoundly reshaped the acquisition of human knowledge and shown impressive language reasoning capabilities, *i.e.*, Symbol-LLM framework. In Sec. 3.2.1 and Sec. 3.2.2, we discuss the approximation of the two ideal properties with the help of LLMs and provide practical solutions, then a summarized pipeline is presented in Sec. 3.2.3.

3.2.1 Solving Semantic Coverage

Approximation. In Def. 5, the target domain of semantic coverage is a very large-scale activity image database, which is too costly to implement. For instance, HAKE [28] collect symbols from 100 K+ image via manual annotations, which is a heavy workload but still very limited. Here, the target domain can be replaced with semantic coverage of language models since natural language is another carrier of human commonsense knowledge. LLMs profit from large-scale text pre-training and imply abundant text-based human knowledge, thus can handle complex visual activity patterns without extra visual data. The approximation of Def. 5 is:

Definition 7. (Approximation of Semantic Coverage of Activity Symbolic System) Given an LLM \mathcal{L} and an activity set $\mathcal{A}, \forall A \in \mathcal{A}, \mathcal{L}$ implies a symbol set \mathcal{S}_A as premises of A , then $\forall s \in \mathcal{S}_A, s \in \mathcal{S}$.

Symbol-Rule Loop. In the implementation, generating rules connecting the symbols is non-trivial and challenging. Intuitively, we can ask LLMs “What is the rule of the activity”. However, the instruction is ambiguous for LLMs to generate satisfying answers. More information should be provided to generate rules. Also, it is costly to generate all symbols and exhaustively query their connections. Thus, we propose to adopt *symbol-rule loops* to generate them alternately. Given a known symbol, we can add another symbol and extend it into a rule via prompting:

(Rule Extension)

In a picture, IF [`<known symbols>`] AND [`<condition>`] THEN [`<activity>`].
 [`<condition>`] is one concise phrase. The format is "`<The person's hands/arms/hip/legs/feet> <verb> <object>`". What is [`<condition>`]?"

Then, the answer for “[code><condition>]” is the extended symbol. Also, a candidate rule “`<known symbols> \wedge <extended symbol> \models <activity>`” is generated. Thus, we get a new extended symbol from this known symbol, and they are connected with rules. The new symbol can be repeatedly used as a known symbol to generate new rules. As is shown in Fig. 2b, a known symbol (the brown circle) is first “popped out” from a queue, and new symbols (the green circle) and rules (the pink edge) are generated by extending the known symbol. Then, the new symbol is “pushed in” to start the next loop. Thus, LLMs’ implicit knowledge is fully exploited to satisfy Def. 7. To get the initial symbols, we ask an LLM to describe hand-related states related to the activity. The prompts mentioned above are determined via a trial-and-error process by human experts on randomly sampled activities (detailed in supplementary).

3.2.2 Solving Logical Entailment

Approximation. In Def. 6, it is costly to verify the logical entailment upon a very large-scale activity image database. Instead, we develop an entailment scoring function from an LLM based on its knowledge and language reasoning capability. As illustrated in Fig. 2c, as the rule extends from $m_1 \models c$, $m_1 \wedge m_2 \models c$ to $m_1 \wedge m_2 \wedge m_3 \models c$, new symbols are successively added, and the measured entailment score increases. With the scoring function, the approximation of Def. 6 is:

Definition 8. (Approximation of Logical Entailment of Activity Symbolic System) Given a function $\tau(\cdot)$ to measure the entailment score of a rule, and an entailment threshold e_h , then $\forall r = (M, C) \in \mathcal{R}$, $M = \{m_i\}_{i=1}^{n_r}$, we have:

1. $\tau(\bigwedge_{m \in M} m \models c) \geq e_h$;
2. $\forall 1 \leq i \leq n_r$, $\tau(\bigwedge_{m \in M \setminus \{m_i\}} m \models c) < e_h$.

Entailment Check. As is shown in Fig. 2c, to implement the scoring function based on an LLM, we rewrite the rule r as a sentence and design the prompt as:

(Entailment Check)

In a picture, `<symbol 1>`, `<symbol 2>` ... `<symbol n_r >`. Estimate the probability that he is `<activity>` at the same time. Choose from: (a) 0.1, (b) 0.5, (c) 0.7, (d) 0.9, (e) 0.95, (f) unknown.

Then, the output answers can be used as the entailment score $e = \tau(r)$, whose credibility depends on the knowledge from the LLM. For one rule, the answering text is sampled five times and their average scores are taken as the final result to add stability. In practice, we set $e_h = 0.9$.

3.2.3 Summarized Pipeline

The pipeline of the symbolic system can be summarized as: given a target activity set \mathcal{A} , or equivalently, a conclusion set \mathcal{C} , we generate a sub-system $(\mathcal{S}_c, \mathcal{R}_c)$ for each $c \in \mathcal{C}$ (Def. 4). The symbolic system is merged as $(\mathcal{S}, \mathcal{R}) = (\bigcup_{c \in \mathcal{C}} \mathcal{S}_c, \bigcup_{c \in \mathcal{C}} \mathcal{R}_c)$. Alg. 2 shows how to get the sub-system $(\mathcal{S}_c, \mathcal{R}_c)$ for a given conclusion c . Details are explained in Alg. 2 comment and the supplementary.

3.3 Reasoning with Visual Inputs

With the activity symbol system constructed, we can utilize it to reason with visual inputs. As is shown in Fig. 3, visual information is extracted and checked based on the defined symbols and

Algorithm 1 Instantiating the Symbolic System

Input: conclusion c , entailment threshold e_h
Output: Symbolic Sub-System $(\mathcal{S}_c, \mathcal{R}_c)$

```

1:  $\mathcal{S}_c^0 \leftarrow \text{Symbol\_Initialization}(c)$ 
2:  $\mathcal{S}_c^{\text{cand}}.\text{push}(\mathcal{S}_c^0)$  ▷ A queue  $\mathcal{S}_c^{\text{cand}}$  stores symbols
3:  $\mathcal{S}_c \leftarrow \{c\}, \mathcal{R}_c \leftarrow \{\}$ 
4: while not  $\mathcal{S}_c^{\text{cand}}.\text{is\_empty}()$  do
5:    $m_{\text{kno}} \leftarrow \mathcal{S}_c^{\text{cand}}.\text{pop}()$  ▷ A known symbol  $m_{\text{kno}}$  is taken for rule extension
6:    $M = \{m_{\text{kno}}\}$  ▷ The premises set  $M$  is set for the current rule
7:   while  $\text{Entailment\_Check}(M) < e_h$  do
8:      $m_{\text{new}} \leftarrow \text{Rule\_Extension}(M, c)$ 
9:      $M = M \cup \{m_{\text{new}}\}$  ▷ A new symbol  $m_{\text{new}}$  is added
10:  end while
11:   $\mathcal{S}_c \leftarrow \mathcal{S}_c \cup M$  ▷ The symbol set  $\mathcal{S}_c$  is updated
12:   $\mathcal{R}_c \leftarrow \mathcal{R}_c \cup \{r : \bigwedge_{m \in M} m \models c\}$  ▷ The rule set  $\mathcal{R}_c$  is updated
13:   $\mathcal{S}_c^{\text{cand}}.\text{push}(M \setminus \mathcal{S}_c)$  ▷  $M$  is added to  $\mathcal{S}_c^{\text{cand}}$  with redundant symbols removed
14: end while
15: return  $(\mathcal{S}_c, \mathcal{R}_c)$ 

```

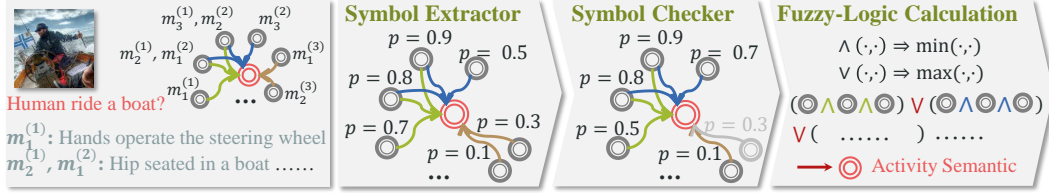


Figure 3: Visual reasoning with the proposed activity symbol system.

organized as a probability distribution on the hyper-graph. Then, the activity semantics can be reasoned out based on the rules and the probability of the symbols. We detail the key steps as follows.

Decomposition. Given the input image and the target activity/conclusion c , we first decompose the symbol system to exclude unrelated symbols and rules based on Def. 4. Thus, we get the rule set $\mathcal{R}_c = \{r^{(j)}\}_{j=1}^{N_c}$, where a rule takes the form $r^{(j)} : m_1^{(j)} \wedge m_2^{(j)} \wedge \dots \wedge m_{n_r(j)}^{(j)} \models c$.

Extracting Visual Symbols. Given an image, to extract visual content and express it in a symbolic form, we measure the probability of each defined symbol (Fig. 3). In [26], the visual extractor is a customized model trained with annotations, which is costly, especially for our symbolic system with broad-range symbols. Instead, we utilize a simplified visual extractor based on existing System-1-like VLMs. To determine the probability of a symbol, we convert it into a text question and query the answer from a VLM. For example, given a premise symbol $m_i^{(j)}$ “Hip seated in a boat”, it is converted into a sentence “The person’s hip is seated in a boat. Yes/No?”. Used as a scoring function [1], the language model outputs the probability of answering “Yes”, “No” as $p_{y,i}^{(j)}, p_{n,i}^{(j)}$. Then the probability $p_i^{(j)}$ of the symbol can be obtained via normalizing the Yes/No answer as

$$p_i^{(j)} = \frac{e^{p_{y,i}^{(j)}}}{e^{p_{y,i}^{(j)}} + e^{p_{n,i}^{(j)}}}. \quad (1)$$

Checking Visual Symbols. To ensure the reliability of the symbols’ probabilities, we developed a checker module to filter out visual symbols with uncertain predictions. Each symbol is paraphrased into several variants, and the predictions of variants should be similar due to semantic consistency. Thus, the standard deviation of the predictions can be used to filter symbols with uncertainty.

Reasoning. With the symbol extractor and checker, the probability $p_i^{(j)}$ for each premise symbol $m_i^{(j)}$ in the rule set \mathcal{R}_c is measured. Then, the probability p_c of the conclusion is reasoned based on premise symbols’ probabilities and the rules. Premise symbols within a rule are connected with \wedge , while rules for a conclusion are connected with \vee . We utilize the fuzzy-logic calculation [46], where

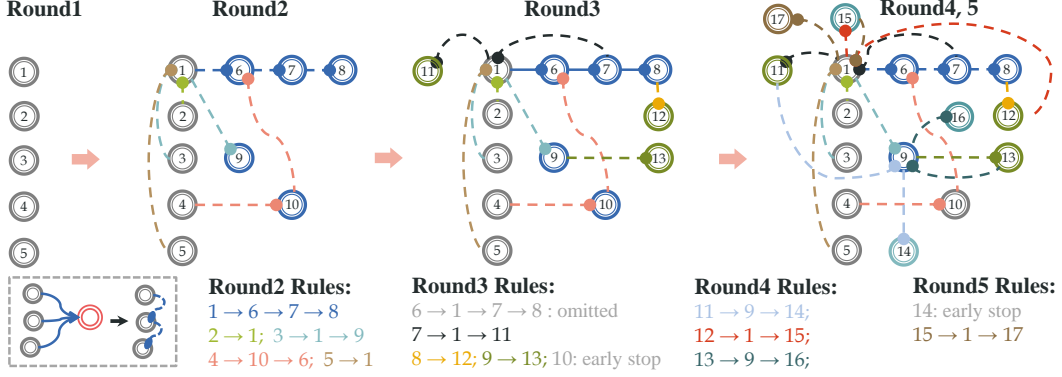


Figure 4: Detailed process for instantiating the symbolic sub-system of the activity “Human board an airplane”. As is shown in the left bottom box, there is some difference in graph presentation between this figure and Fig. 1-3: here the edge connects premises instead of connecting premise and conclusion. The numbers 1-17 correspond to the 17 symbols listed in Tab. 1. The “ \rightarrow ” in “ $1 \rightarrow 6 \rightarrow 7 \rightarrow 8$ ” means that 6, 7, 8 is obtained via 1’s rule extension one after another.

| | Symbols | |
|---------------|---|---|
| Round1 | (1) hold a boarding pass | (2) place luggage in overhead compartment |
| | (3) adjust seatbelt | (4) wave goodbye to loved ones |
| Round2 | (5) grip a luggage handle | |
| | (6) walk towards the boarding gate | (7) luggage visible beside him |
| | (8) boarding pass is scanned by airport staff | (9) stand on the jet bridge |
| Round3 | (10) luggage is loaded onto the plane | |
| | (11) reach for the airplane door handle | (12) stand in line with carry-on luggage |
| Round4 | (13) hold the carry-on luggage | |
| | (14) open the airplane door | (15) move forward in the line |
| Round5 | (16) move towards the airplane door | |
| | (17) airline staff checking the boarding pass | |

Table 1: Generated symbols & rules for “human board an airplane”. Round i : i -th symbol-rule loop.

the operator $x \wedge y, x \vee y$ are replaced with $\min(x, y), \max(x, y)$ respectively. Thus, we have

$$p_c = \max_{1 \leq j \leq N_c} (\min_{1 \leq i \leq n_r(i)} p_i^{(j)}). \quad (2)$$

The fuzzy-logic calculation is more explainable and lightweight than the logical modules in [26], whose parameters need extra training samples. Benefiting from the sound definition of our symbolic system, it has the potential to achieve *better* performance even with simplified reasoning calculations.

4 Experiment

4.1 Dataset and Metric

We conduct experiments on image-level activity understanding benchmarks with diverse tasks: **HICO** [5] (Human-Object Interaction (HOI) recognition), **Stanford40** [44] (action recognition), **HAKE [28]-Verb** (verb recognition), **HAKE [28]-PaSta** (conditional PaSta Q-A). HAKE [28]-Verb and HAKE [28]-PaSta is the newly constructed benchmark based on HAKE [28] data. We adopt mAP metric for HICO [5], HAKE [28]-Verb and Stanford40 [44], and top-1 accuracy metric for HAKE [28]-PaSta. For more details, please refer to the supplementary.

4.2 Symbolic System Experiment

An example. The LLM used is OpenAI GPT3.5. To demonstrate the instantiation of our symbolic system, we take the activity “human board an airplane” as an example. Tab. 1 shows the symbols and rules generated, and Fig. 4 illustrates the detailed process. In the 1st round, 5 initial symbols are generated. Then in the 2nd round, they are extended into rules satisfying entailment. Later, the new symbols are used in the next round. Finally, 17 symbols and 12 rules are generated within 5

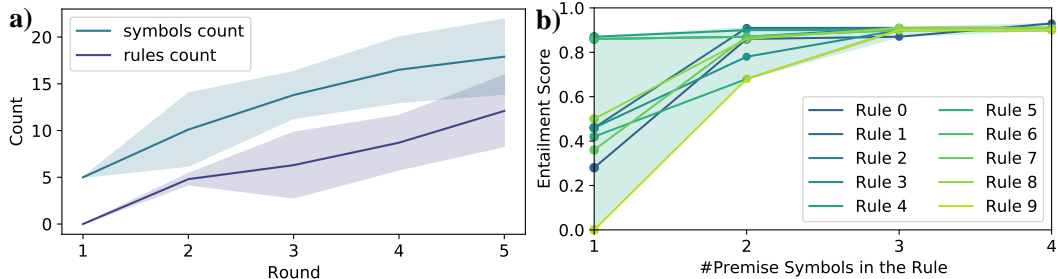


Figure 5: Statistics of the symbolic system. a) Accumulated symbols & rules count in each round. The data is from 50 randomly sampled activities. The average value and fluctuation range are shown. b) Increased entailment scores as the 10 randomly sampled rules extended with more premise symbols.

rounds. In practice, at most 15 symbols are used for rule extension to avoid semantic redundancy. For example, in Fig. 4, symbols 16 and 17 are not used for rule extension, leading to a stop in the 5th round. From Fig. 4 and Tab. 1, we can find that diverse symbols are mined, including corner cases such as “adjust seatbelt” “reach for the airplane door handle”, verifying the effectiveness of the proposed symbolic system. Some special cases are shown as gray text. The rule “ $6 \rightarrow 1 \rightarrow 7 \rightarrow 8$ ” is equivalent to the existing rule “ $1 \rightarrow 6 \rightarrow 7 \rightarrow 8$ ”, thus omitted. Extension from the symbols 10 and 14 stops early because adding premises nevertheless leads to a drop in entailment scores. In practice, multiple rules are extended from a known symbol to increase diversity.

Entailment. Fig. 5 shows statistics of the symbolic system. In Fig. 5a, we randomly sample 50 activities and show the accumulated symbols and rules count in each round, verifying the diversity of the generated symbols and rules. In Fig. 5b, we randomly sample 10 rules and show the entailment scores change as the rule extends with more premise symbols. For example, for rule 0: $m_1 \wedge m_2 \wedge m_3 \wedge m_4 \models c$, the entailment score for $m_1 \models c$, $m_1 \wedge m_2 \models c$, $m_1 \wedge m_2 \wedge m_3 \models c$, $m_1 \wedge m_2 \wedge m_3 \wedge m_4 \models c$ are 0.28, 0.86, 0.87, and 0.93, respectively. The score is calculated by querying 5 times and averaged. We find a climb up in the entailment score, implying the effectiveness of the entailment check. Once the entailment score e surpasses the threshold $e_h = 0.9$, it is regarded as a rule equipped with logical entailment and updated into the symbolic system.

Performance Evaluation. To evaluate the symbolic system, we construct a SymAct (Symbol Activity) test set. It is a small subset of the HICO test set (120 images for 10 activity classes). For each image and each of its ground-truth activities, we list all of the symbols related to the activity in the symbolic system and annotate whether a symbol happens (0/1) in the image via human judgment. We find the proposed symbolic system has: **1) broader semantic coverage** than HAKE. For quantitative measurement, we count the happening symbols for each image-activity pair under different symbolic systems. The average number is 10.8 for ours and 1.8 for HAKE. **2) more rational rules** than HAKE. We evaluate confusion by counting different image-activity pairs which share the same symbols. For the HAKE symbolic system, the confusion problem is severe, with 261 confusion pairs over $C_{120}^2 = 7140$ pairs (accounting for 3.7%). For our symbolic system, there are no confusion pairs on the test set because of the presentation ability of symbols and entailment check.

Robustness. We analyze the robustness of the generated symbolic system. We find it satisfies: **1) Convergence.** After a certain stopping criterion, a new round will bring few or even no new symbols to the sub-system. In practice, the stopping criterion is: At most 15 symbols are used for rule extension to avoid semantic redundancy. After that, new symbols are not used for rule extension, leading to a stop of the loop. **2) Low sensitivity to initial conditions.** The symbol-rule loop provides a reliable and stable symbolic sub-system over a range of initial conditions. **3) Low sensitivity to different prompts.** Experiment results are less sensitive to prompts with minor differences, *i.e.*, slightly paraphrasing the prompts. For more details, please refer to the supplementary.

4.3 Visual Reasoning Experiment

Implementation and Settings. For visual reasoning, we use BLIP2 [24] ViT-g FlanT5-XL model to extract visual symbols. BLIP2 [24] is a visual-language pre-trained model with a frozen large language model, thus well equipped with question-answering abilities to effectively extract symbols.

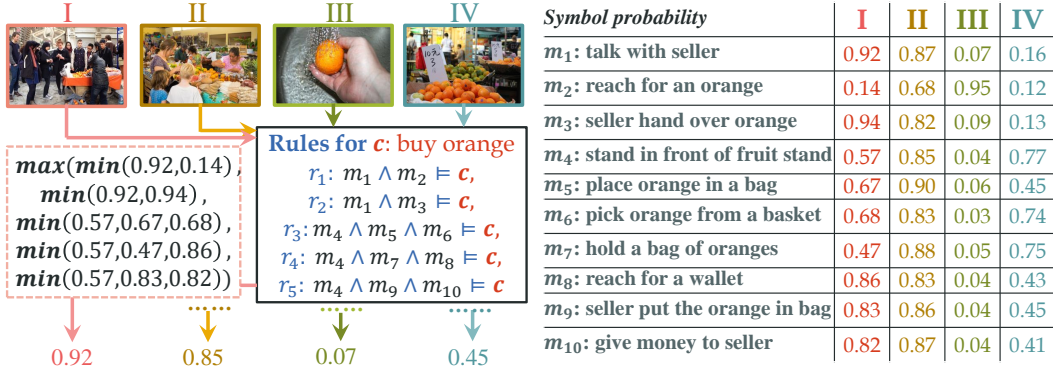


Figure 6: Visualization results. Symbols & activity predictions for “human buy orange” are shown.

| Method | HICO mAP | | HAKE-verb mAP | | Stanford-40 zero-shot mAP | HAKE-PaSta zero-shot Acc (%) |
|----------------------|--------------|--------------|---------------|--------------|---------------------------|------------------------------|
| | fine-tuned | zero-shot | fine-tuned | zero-shot | | |
| CLIP [37] | 67.12 | 37.08 | 73.82 | 43.92 | 75.68 | 39.36 |
| CLIP [37]+Reasoning | 69.73 | 43.21 | 75.27 | 48.95 | 82.22 | 40.47 |
| BLIP2 [24] | - | 50.61 | - | 49.47 | 91.85 | 43.81 |
| BLIP2 [24]+Reasoning | - | 53.15 | - | 51.37 | 92.59 | 44.65 |

Table 2: Results on activity benchmarks. More HICO [5] baselines are listed in supplementary.

As a *plug-and-play*, the reasoning is compatible with existing System-1-like methods. We follow the setting of HAKE [26] to integrate the reasoning result with the prediction of System-1-like methods. We mainly choose 2 typical System-1-like methods: 1) CLIP [37]: a visual-language model pre-trained with large-scale image-text pairs and a contrastive objective, where we use its ViT-L/14 model with a resolution of 336 pixels; 2) BLIP2 [24]: with its image-to-text generation ability, it functions either as a System-1-like baseline, or as the symbol extractor for reasoning. To fully test the ability of the models, we adopt both “fine-tuned” and “zero-shot” settings, where the former model is fine-tuned on the training set of the dataset.

Results. The results of visual reasoning are shown in Tab. 2. Comparing the two baselines, we find that with a frozen language model, BLIP2 [24] is more capable of understanding activity semantics and outperforms CLIP [37] in various zero-shot benchmarks. Under the fine-tuned setting, our method achieves **69.73** and **75.27** mAP respectively on HICO [5] and HAKE [28]-Verb, which outperforms the baseline CLIP [37] with **2.61** and **1.45** mAP respectively, verifying its effectiveness. Under the zero-shot setting, our method also outperforms existing System-1-like methods. The improvement compared with CLIP [37] is: **6.13** mAP (HICO [5]), **5.03** mAP (HAKE [26]-Verb), **6.54** mAP (Stanford40 [44]), **1.11%** acc (HAKE [26]-PaSta). The improvement compared with BLIP2 [24] is: **2.54** mAP (HICO [5]), **1.90** mAP (HAKE [26]-Verb), **0.74** mAP (Stanford40 [44]), **0.84%** acc (HAKE [26]-PaSta). In conclusion, our method brings performance improvement and shows significant zero-shot *generalization* abilities in various activity understanding tasks. Notably, the improvement is achieved by exploiting knowledge instead of adding visual training samples. The exploited knowledge can be reused for future study. Thus, our method is superior in *data efficiency*. Further, we visualize the results in Fig. 6. The rules and the logic calculation add *explainability* to the inference process. Also, they help to correct false negative (I, II in Fig. 6) and false positive (III, IV) cases, thus improving compositional generalization.

4.4 Ablation Study

We conduct ablation studies on HAKE [26]-Verb zero-shot setting and list the results in Tab. 3.

Reasoning. We first verify the effectiveness of integrating System-2 reasoning. Results of CLIP [37] baseline can be either combined with reasoning results or trivially combined with other baseline results (CLIP [37]+BLIP2 [24]). We find that the former is superior (48.95 mAP) to the latter (44.76 mAP), though both outperform the baseline CLIP [37] (43.92 mAP). It verifies the necessity of System-2 reasoning other than trivially combining predictions from two models.

Symbolic System. We then verify the effects of the symbolic system on visual reasoning. We adopt the symbolic system in HAKE [26] and find a degradation from 48.95 to 44.98 mAP, as its defects in semantic coverage and rule rationality, and the shortage is amplified in the fuzzy logic calculation without learnable parameters. Next, we construct the symbolic system without logical entailment, where each rule has 3 premise symbols without checking its entailment score. It leads to a dropped performance because of rules with errors or incomplete semantics. Then, the symbol-rule loop is removed, with only rules in the 1st and 2nd rounds updated to the symbolic system. As the diversity of rules decreases, the model suffers from a decreased performance. The importance of diversity is further verified by the performance drop when only 80%, 50%, and 20% randomly sampled rules are used.

| Method | mAP |
|------------------------|--------------|
| CLIP [37]+Reasoning | 48.95 |
| CLIP [37]+BLIP2 [24] | 44.76 |
| CLIP [37] | 43.92 |
| rules from HAKE [26] | 44.98 |
| w/o entailment check | 46.51 |
| w/o symbol-rule loop | 47.53 |
| 80% rules | 48.57 |
| 50% rules | 47.61 |
| 20% rules | 46.22 |
| CLIP [37] as extractor | 46.09 |
| w/o checking symbols | 48.17 |

Table 3: Ablation studies on zero-shot HAKE [26]-Verb.

Symbols Extractor/Checker. Next, we replace the symbol extractor BLIP2[24] with CLIP [37] and find a performance fall with a weaker ability to extract visual information. Also, reasoning without a symbol checker suffers from degradation due to the negative effect of inaccurate symbol predictions.

4.5 Bottleneck Analysis

Based on the SymAct test set, we make further analysis of the bottleneck of System-2 reasoning. We investigate the impact of symbol prediction and symbolic system separately. With perfect symbol predictions, we assume the probabilities of symbols are definitely known as 0/1 instead of $p \in [0, 1]$. The ground-truth symbols are annotated as explained in Sec. 4.2. With a perfect symbolic system, we assume that the generated rules cover all samples (image-activity pairs). The performance drop (100.00→60.79 mAP, 83.11→41.52 mAP) indicates the symbolic system errors, *i.e.*, the generated rules have not covered all samples (image-activity pairs). The drop (100.00 → 83.11 mAP, 60.79 →41.52 mAP) indicates the errors of symbol predictions, *i.e.*, symbol probabilities cannot be predicted accurately. In the supplementary, we also provide two failure cases that emerge from symbol prediction errors and symbolic system errors respectively.

| Symbol Prediction | Symbolic System | mAP |
|-------------------|-----------------|---------------|
| perfect | perfect | 100.00 |
| imperfect | perfect | 83.11 |
| perfect | imperfect | 60.79 |
| imperfect | imperfect | 41.52 |

Table 4: System-1/2 analysis on SymAct test set.

5 Conclusion and Discussion

In this work, we rethink the symbolic system in activity reasoning and propose a new one with broad-coverage symbols and rational rules. Thus, enhanced System-2 reasoning is integrated into System-1. We demonstrate how to instantiate it and how it helps to reason with visual inputs. Our method shows superiority in explainability, generalization, and efficiency in extensive experiments.

Computation Cost. Symbol predictions will increase the computational cost as a trade-off for explainability and generalization. It can be eased by discovering the hierarchical and reusable nature of the symbols, which is detailed in the supplementary.

Broader Application. The method could be more general and facilitate real-world applications. We choose activity understanding as a good and important initial test bed because it is a difficult task with complex visual patterns and a compositional nature. To verify the broader application, we provide some initial results on object recognition and VCR [47] tasks in the supplementary.

Limitation. Rules generated from language models mostly boost System-1, but sometimes bring language bias, *e.g.*, the person only decides to buy an orange despite apples in the background. Further, the approximation is mainly based on pre-trained LLMs and can be improved with more elaborate designs, *e.g.*, human-in-the-loop, customized LLMs with higher-quality knowledge. Besides, System-2 reasoning may be boosted if integrated into the System-1 training process. Also, instance-level activities and temporal encoding are beyond our scope since our main focus is on an overall framework to formulate and construct a novel symbolic system. We leave them to future work.

Acknowledgments and Disclosure of Funding

Some of the drawing materials in Fig. 1,2 are designed by Layerace / Freepik.

This work is supported in part by the National Natural Science Foundation of China under Grants 62306175, National Key R&D Program of China (No.2021ZD0110704), Shanghai Municipal Science and Technology Major Project (2021SHZDZX0102), Shanghai Qi Zhi Institute, Shanghai Science and Technology Commission (21511101200).

Appendix

A Notations

In Tab. 5, we conclude the notations in this work for clarity.

| Notation | Definition |
|----------------------------------|--|
| r | A rule. It takes the form $r : m_1 \wedge m_2 \wedge \dots \wedge m_{n_r} \models c$. |
| $M = \{m_i\}_{i=1}^{n_r}$ | The premise symbols set of the rule r . |
| c | The conclusion symbol of the rule r . |
| n_r | The size of the premise symbols set M . |
| \wedge | Logic AND. |
| \vee | Logic OR. |
| \models | Entailment. |
| $(\mathcal{S}, \mathcal{R})$ | The activity symbolic system. \mathcal{S} is the symbol set, and \mathcal{R} is the rule set. |
| $(\mathcal{S}_c, \mathcal{R}_c)$ | The activity symbolic sub-system given a conclusion c . |
| $A \setminus B$ | The set difference of A and B. |
| \mathcal{D} | A very large-scale activity images database. $\mathcal{D} = \{(I, A, \mathcal{S}_I)\}$. |
| I | An image. |
| A_I | The activities happening in an image I . |
| \mathcal{S}_I | Ongoing symbols in an image I . |
| \mathcal{L} | An LLM. |
| \mathcal{A} | The activity set contains multiple activity classes. $\mathcal{A} = \{A\}$ |
| \mathcal{C} | The conclusion set contains multiple conclusions. \mathcal{A} and \mathcal{C} is equivalent. |
| \mathcal{S}_A | The premise symbols set for activity A . It is implied from an LLM. |
| e | The entailment score of a rule. |
| e_h | The entailment score threshold to accept/reject a rule. We set $e_h = 0.9$. |
| $\tau(\cdot)$ | A function to measure the entailment score $e = \tau(r)$ of a rule r . |
| $r^{(j)}$ | The j -th rule in \mathcal{R}_c . It takes the form $r^{(j)} : m_1^{(j)} \wedge m_2^{(j)} \wedge \dots \wedge m_{n_r^{(j)}}^{(j)} \models c$. |
| $m_i^{(j)}$ | The i -th premise symbol in the j -th rule of \mathcal{R}_c . |
| $p_{y,i}, p_{n,i}^{(j)}$ | The output probability of answering "Yes""No" for the symbol $m_i^{(j)}$ from a VLM. |
| $p_i^{(j)}$ | The probability of the symbol $m_i^{(j)}$. |
| $N_{query,c}$ | The number of queries to generate the symbolic sub-system given the conclusion c . |
| N_{ent} | The number of sampling to calculate the entailment score. $N_{ent} = 5$. |
| $ M^{(j)} $ | The size of the premise symbol set for a rule $r^{(j)}$. |
| $\{m_{i,k}^{(j)}\}_{k=1}^5$ | The paraphrased variants for the symbol $m_i^{(j)}$. |
| $\{p_{i,k}^{(j)}\}_{k=1}^5$ | The probability of the symbols $\{m_{i,k}^{(j)}\}_{k=1}^5$. |
| $std_i^{(j)}$ | The standard deviation of $\{p_{i,k}^{(j)}\}_{k=1}^5$. |
| \mathcal{S}_{sys1} | The prediction of a System-1-like method. |
| \mathcal{S}_{sys2} | The prediction of a System-2-like method. |
| \mathcal{S}_{int} | The final integrated prediction. |
| α_1, α_2 | The re-scaling factors to normalize $\mathcal{S}_{sys1}, \mathcal{S}_{sys2}$. |

Table 5: Notations and their definition of this work.

About the entailment notation. We replace the notation " \rightarrow " in HAKE with " \models " for mathematical rigor. The notations " \models " (semantic entailment) and " \rightarrow " (logical/syntactic entailment) both describe the concept of one statement leading to another, but their emphasis is different. Semantic entailment

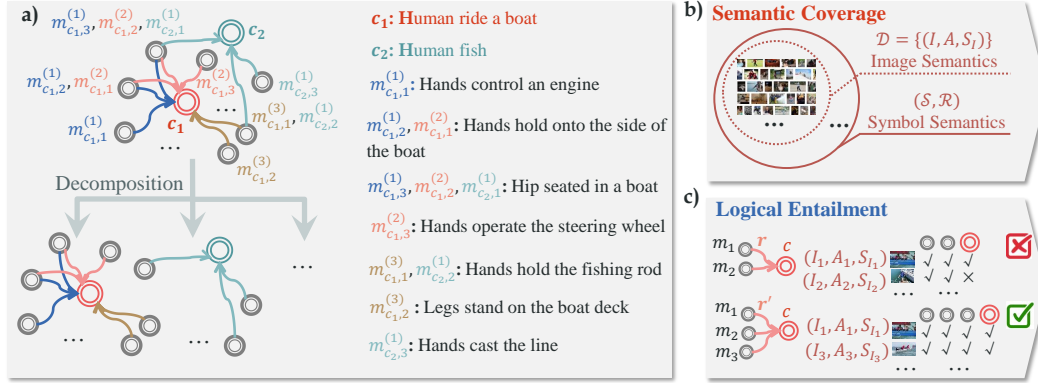


Figure 7: Our activity symbolic system. a) The structure and decomposition. Its two important properties: b) semantic coverage and c) logical entailment. It details part of Fig. 2 in the main text.

focuses on the reasoning relationship based on truth values or interpretations. When all interpretations that make all formulas in A true also make B true, we say that A semantically entails B . Syntactic entailment focuses on the ability to derive a conclusion from a set of premises based on formal reasoning rules. When Q can be derived from the formulas in P solely through reasoning rules, we say that P syntactically entails Q . Semantic entailment focuses on truth tables or interpretations (*i.e.*, under what circumstances or "worlds" a proposition is true), while syntactic entailment focuses on formal reasoning rules and proof processes. Visual reasoning focuses on interpretations instead of syntactic proof. Thus we replace the notation " \rightarrow " in HAKE with " \models ".

B More Details of Symbolic System Formulation

B.1 Explanation of the Illustration

In the main text, Fig. 2 illustrates the overview of the proposed activity symbolic system. We give a more detailed explanation here. This section focuses on the part of Fig. 2 related to the symbolic system formulation. The other parts are left to Sec. C.1.

Fig. 7a explains the structure and decomposition of our activity symbolic system. The premise symbols (gray circles), the conclusion symbols (red and green circles), and the rules (blue, red, brown, and green edges) are shown. Example meanings of symbols are also listed. When decomposing the activity symbolic system into sub-systems, unrelated symbols/rules are removed within each sub-system. Fig. 7b explains the semantic coverage property, *i.e.*, comparing the image semantics in the database \mathcal{D} and symbol semantics in the symbolic system $(\mathcal{S}, \mathcal{R})$. Fig. 7c explains the logical entailment property. The rule $r: m_1 \wedge m_2 \wedge m_3 \models c$ satisfies logical entailment, while $r': m_1 \wedge m_2 \not\models c$ fails because in (I_2, A_2, S_{I_2}) , $\{m_1, m_2\} \subset S_{I_2}$ but $c \notin A_2$.

B.2 Asymmetry of Rule

In Sec. 3.1.1 in the main text, we analyze the structure of the symbolic system as a type of directed hyper-graph instead of the indirect hyper-graph. This is because of the asymmetry of the rule: within one rule, the premises symbol and the conclusion symbol cannot swap positions. That is, for a rule $r: m_1 \wedge m_2 \wedge \dots \wedge m_{n_r} \models c$, another rule $r': m_1 \wedge \dots \wedge m_{i-1} \wedge c \wedge m_{i+1} \wedge \dots \wedge m_{n_r} \models m_i$, ($1 \leq i \leq n_r$) is not necessarily satisfied. For example,

$$\begin{aligned}
 r: & \text{ Hip seated in a boat } \wedge \text{ Hand hold onto the side of the boat } \wedge \text{ Hand} \\
 & \text{ operate the steering wheel } \models \text{ Human ride a boat} \\
 r': & \text{ Hip seated in a boat } \wedge \text{ Hand hold onto the side of the boat } \wedge \text{ Human ride} \\
 & \text{ a boat } \models \text{ Hand operate the steering wheel}
 \end{aligned}$$

The rule r' is not satisfied since there are other possible conclusions, *e.g.*, "Hand controls the engine". Based on the asymmetry property of the rule, the activity symbolic system is defined

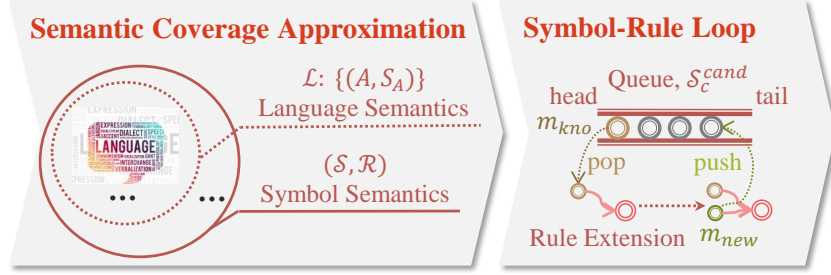


Figure 8: Semantic coverage can be approximated based on LLMs’ knowledge and achieved via the symbol-rule loop. It details part of Fig. 2 in the main text.

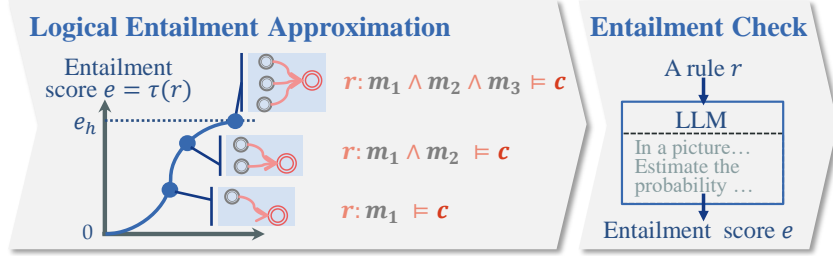


Figure 9: Logical entailment can be approximated based on an entailment scoring function and achieved by entailment check. It details part of Fig. 2 in the main text.

based on a directed hyper-graph, with the edges pointing from the premise symbols to the conclusion symbol.

B.3 Structure of the Previous Symbolic System

Existing methods [28, 26] can also be formulated under the structure in Def. 3 in the main text. Their symbolic system is a specific example of Def. 3, where the premise set M for each rule r is the subset of the hand-crafted activity primitives, *i.e.*, $M \subset M^*$, $|M^*| = 76$ and M^* is a fixed set.

C More Details of Symbolic System Instantiation

C.1 Explanation of the Illustration

We further explain the other part of Fig. 2 in the main text. As is shown in Fig. 8, semantic coverage can be approximated by comparing the symbol semantics in the symbolic system $(\mathcal{S}, \mathcal{R})$ with the LLM semantics implying the premise symbols set S_A for an activity A . In each symbol-rule loop, a known symbol m_{kno} is taken from the queue \mathcal{S}_c^{cand} , and the rule extension is applied with a new symbol m_{new} added. As is shown in Fig. 9, the logical entailment is measured via an entailment scoring function $\tau(\cdot)$. For the rule $r : m_1 \wedge m_2 \wedge m_3 \models c$, the entailment score for $m_1 \models c, m_1 \wedge m_2 \models c, m_1 \wedge m_2 \wedge m_3 \models c$ climbs up because more premise symbols are added. Once the entailment score e surpasses the threshold e_h , it is regarded as a rule equipped with logical entailment and updated into the symbolic system. To implement the scoring function based on an LLM, we rewrite a rule r as a sentence and design prompts.

C.2 Summarized Pipeline

Alg. 2 in the main text shows how to get the sub-system $(\mathcal{S}_c, \mathcal{R}_c)$ for a given conclusion c . We again show it in this supplementary and explain it for clarity. The target is to determine the rule set $\mathcal{R}_c = \{r^{(j)}\}_{j=1}^{N_c}$, where a rule takes the form $r^{(j)} : m_1^{(j)} \wedge m_2^{(j)} \wedge \dots \wedge m_{n_r^{(j)}}^{(j)} \models c$, or equivalently, $r^{(j)} : \bigwedge_{m \in M^{(j)}} m \models c$. Correspondingly, the symbol set is $\mathcal{S}_c = (\bigcup_{j=1}^{N_c} M^{(j)}) \cup \{c\}$.

Algorithm 2 Instantiating the Symbolic System

Input: conclusion c , entailment threshold e_h **Output:** Symbolic Sub-System $(\mathcal{S}_c, \mathcal{R}_c)$

```
1:  $\mathcal{S}_c^0 \leftarrow \text{Symbol\_Initialization}(c)$ 
2:  $\mathcal{S}_c^{cand}.push(\mathcal{S}_c^0)$  ▷ A queue  $\mathcal{S}_c^{cand}$  stores symbols
3:  $\mathcal{S}_c \leftarrow \{c\}, \mathcal{R}_c \leftarrow \{\}$ 
4: while not  $\mathcal{S}_c^{cand}.is\_empty()$  do
5:    $m_{kno} \leftarrow \mathcal{S}_c^{cand}.pop()$  ▷ A known symbol  $m_{kno}$  is taken for rule extension
6:    $M = \{m_{kno}\}$  ▷ The premises set  $M$  is set for the current rule
7:   while  $\text{Entailment\_Check}(M) < e_h$  do
8:      $m_{new} \leftarrow \text{Rule\_Extension}(M, c)$ 
9:      $M = M \cup \{m_{new}\}$  ▷ A new symbol  $m_{new}$  is added
10:  end while
11:   $\mathcal{S}_c \leftarrow \mathcal{S}_c \cup M$  ▷ The symbol set  $\mathcal{S}_c$  is updated
12:   $\mathcal{R}_c \leftarrow \mathcal{R}_c \cup \{r : \bigwedge_{m \in M} m \models c\}$  ▷ The rule set  $\mathcal{R}_c$  is updated
13:   $\mathcal{S}_c^{cand}.push(M \setminus \mathcal{S}_c)$  ▷  $M$  is added to  $\mathcal{S}_c^{cand}$  with redundant symbols removed
14: end while
15: return  $(\mathcal{S}_c, \mathcal{R}_c)$ 
```

First, the initial symbols \mathcal{S}_c^0 are generated (L1 in Alg. 2). For the symbol-rule loop (L4-14), a queue \mathcal{S}_c^{cand} stores candidate symbols, and each loop processes one symbol m_{kno} in \mathcal{S}_c^{cand} . In each loop, a known symbol m_{kno} is taken as an element in the premise symbol set M , and the rule extension is repeatedly applied with the new symbol m_{new} added to M until the entailment check is passed (L7-10). Thus, a rule $r : \bigwedge_{m \in M} m \models c$ which satisfies logical entailment is obtained and added to the rule set \mathcal{R}_c (L12). Meanwhile, the new symbols are added to the symbol set \mathcal{S}_c and the candidate symbol set \mathcal{S}_c^{cand} , and the repeated symbols are removed. The symbol-rule loop continues until \mathcal{S}_c^{cand} is emptied. Finally, we get the symbol set \mathcal{S}_c and rule set \mathcal{R}_c for the conclusion c .

C.3 Determining Prompts

The prompts are determined via a trial-and-error process by human experts on randomly sampled 10 activities. Human experts have read the image samples of these activities, and thus have expert knowledge about what symbols/rules are more suitable for visual reasoning. Each round in the trial-and-error process is as follows:

- one expert writes a prompt
- an LLM generates answers by the prompt
- all experts judge whether the answer is suitable
- all experts modify the prompt based on the discovered problems

An example of the trial-and-error process of the prompts for symbol initialization is shown below.

1. Round1:

- Prompt: In a picture, a person is boarding an airplane. What are useful visual features to distinguish his activity?
- Answer: Useful visual features...could include: 1. Luggage: Look for the presence of suitcases, backpacks, or other types of bags that suggest the person is preparing to travel...
- Comment: Object-centric, difficult to extract key information about human activities.

2. Round2:

- Prompt: In a picture, a person is boarding an airplane. What is he doing?
- Answer: The person in the picture is boarding an airplane. Boarding refers to the process of entering the aircraft before the flight begins. It typically involves presenting a valid boarding pass, showing identification, and walking through the designated gate or bridge to reach the plane.

- Comment: Verbose.

3. Round3:

- Prompt: In a picture, a person is boarding an airplane. What is he doing? Answer with 5 concise, highly related phrases. The format is "<human> <verb> <object>".
- Answer: Person boarding airplane.
- Comment: The answer repeats the question.

4. Round4:

- Prompt: In a picture, a person is boarding an airplane. What are his hands doing? Answer with 5 concise, highly related phrases. The format is "<hands> <verb> <object>".
- Answer: 1. Hands holding a boarding pass. 2. Hands placing luggage in overhead compartment. 3. Hands adjusting seatbelt. 4. Hands waving goodbye to loved ones. 5. Hands gripping a luggage handle.
- Comment: Satisfactory.

C.4 An Example of Instantiation

We show the detailed process of generating the symbolic sub-system for the activity “human board an airplane”. It is an extension of the results in Fig. 4, Tab. 1 in the main text, and the method described in Sec. 3.2 in the main text. The LLM used here is OpenAI GPT3.5 via API, where the role is set as “You are helping me understand human activities in a picture.”.

To generate initial premise symbols (L1 in Alg. 2), we prompt as:

(Symbol Initialization)

In a picture, a person is boarding an airplane. What are his hands doing? Answer with 5 concise, highly related phrases. The format is "<hands> <verb> <object>". Output Format: 1. xxx 2. xxx 3. xxx 4. xxx 5. xxx

Then 5 initial symbols are generated from the answer, *e.g.*, “hold a boarding pass”, “place luggage in overhead compartment”.

Then, we extend the symbol “hold a boarding pass” into a rule. To add a new premise symbol (L8 in Alg. 2), we prompt as:

(Rule Extension)

In a picture, there is an airplane. IF [The person is holding a boarding pass.] AND [condition] THEN [The person is boarding the airplane.]. [condition] is one concise phrase. The format is "<The person’s hands/arms/hip/legs/feet> <verb> <object>". What is [condition]? Output Format: [condition] is: [xxx].

With an answer “[condition] is: The person is walking towards the boarding gate”, we get the new symbol “walk towards the boarding gate” and a candidate rule “hold a boarding pass \wedge walk towards the boarding gate \models Human board an airplane”.

Then, an entailment check is applied for the candidate rule (L7 in Alg. 2). The prompt is:

(Entailment Check)

In a picture, there is an airplane. The person is holding a boarding pass. The person is walking towards the boarding gate. Estimate the probability that he is boarding the airplane at the same time. Choose from: (a) 0.1, (b) 0.5, (c) 0.7, (d) 0.9, (e) 0.95, (f) unknown. Output Format: a/b/c/d/e/f.

We sample the answer 5 times and take the average entailment score. If the score $e < e_h$, we repeat the rule extension and entailment check.

(Rule Extension)

In a picture, there is an airplane. IF [The person is holding a boarding pass. The person is walking towards the boarding gate.] AND [condition] THEN [The person is boarding the airplane.] [condition] is one concise phrase. The format is "<The person’s hands/arms/hip/legs/feet> <verb> <object>". What is [condition]?
Output Format: [condition] is: [xxx].

With a new symbol “luggage visible beside him”, the entailment score of the new rule is measured via prompting:

(Entailment Check)

In a picture, there is an airplane. The person is holding a boarding pass. The person is walking towards the boarding gate. The luggage is visible beside him. Estimate the probability that he is boarding the airplane at the same time. Choose from: (a) 0.1, (b) 0.5, (c) 0.7, (d) 0.9, (e) 0.95, (f) unknown. Output Format: a/b/c/d/e/f.

The rule extension and entailment check are repeated until the entailment score threshold is reached. Finally, we get a rule

hold a boarding pass \wedge walk towards the boarding gate \wedge luggage visible beside him \wedge boarding pass is scanned by airport staff \models Human board an airplane

The prompt differences are small modifications necessary to adapt different dataset/task settings. When an interacted object is known, it is listed in the rule extension prompt for emphasis (*e.g.*, "there is an airplane"). For HAKE-PaSta, HOIs are known as conditions, and the symbol initialization is omitted because the known HOIs are initial premise symbols for rule extension.

C.5 Computation Cost

Given a conclusion c , the number of query N_{query} with a LLM is:

$$N_{query,c} = 1 + N_{ent} * \sum_{j=1}^{N_c} |M^{(j)}|, \quad (3)$$

where 1 refers to the first query to generate initial symbols, $N_{ent} = 5$ is the number of sampling to calculate the entailment score, and $|M^{(j)}|$ is the size of the premise symbol set for a rule $r^{(j)}$.

For the example shown in Fig. 4 and Tab. 1 in the main text, we have $N_{query} = 1 + 5 * (4 + 2 + 3 + 3 + 2 + 4 + 3 + 2 + 2 + 3 + 3 + 3 + 3 + 3 + 3) = 216$, where the early stop symbols “10”“14” also need several queries to determine early stop. The exploited knowledge is reusable to facilitate future study.

C.6 Comparing with HAKE

To compare the difference of the symbolic system between our method and HAKE [26], we list some of the rules for the activity “human buy an orange” in Tab. 6. We can see that our symbolic system is superior in semantic coverage and rule rationality.

C.7 Performance Evaluation

To evaluate the symbolic system, we construct a SymAct (Symbol Activity) test set. It is a small subset of the HICO test set (120 images for 10 activity classes). The 10 activity classes are: "human board/wash an airplane", "human park/repair a bicycle", "human feed/race a horse", "human break/sign a baseball bat", and "human buy/wash an orange". These activities have relatively complex visual patterns and cover different interacted objects. For each image and each of its ground-truth activities, we list all of the symbols related to the activity in the symbolic system and annotate whether a symbol happens (0/1) in the image via human judgment.

We find the proposed symbolic system has: **1) broader semantic coverage** than HAKE. For quantitative measurement, we count the happening symbols for each image-activity pair under different symbolic systems. The average number is 10.8 for ours and 1.8 for HAKE. Though a rough estimation, the gap in symbol counts indicates that the symbol semantic of HAKE is limited. Furthermore, in our symbolic system, different activities have different symbols, further boosting semantic coverage. **2) more rational rules** than HAKE. We evaluate confusion by counting different image-activity pairs which share the same symbols. For the HAKE symbolic system, the confusion problem is severe, with 261 confusion pairs over $C_{120}^2 = 7140$ pairs (accounting for 3.7%). For our symbolic system, there are no confusion pairs on the test set because of the presentation ability of symbols and entailment check.

| | | | | | |
|-------------------------------|----------|------------------------------|----------|---------------------------|-----------------|
| talk with seller | \wedge | reach for an orange | - | - | = buy an orange |
| talk with seller | \wedge | seller hand over orange | - | - | = buy an orange |
| stand in front of fruit stand | \wedge | place orange in a bag | \wedge | pick orange from a basket | = buy an orange |
| stand in front of fruit stand | \wedge | hold a bag of oranges | \wedge | reach for a wallet | = buy an orange |
| stand in front of fruit stand | \wedge | seller put the orange in bag | \wedge | give money to seller | = buy an orange |

(a) Rules from our proposed symbolic system.

| | | | | | |
|------------------|----------|---------------------|----------|---|-----------------|
| head: talk to | - | - | - | - | = buy an orange |
| hand: reach for | \wedge | head: inspect | - | - | = buy an orange |
| hand: hold | \wedge | head: smell | - | - | = buy an orange |
| talk with seller | \wedge | reach for an orange | - | - | = buy an orange |
| hand: hold | \wedge | hand: reach for | \wedge | hand: squeeze \wedge head: drink with | = buy an orange |

(b) Rules from the open-source code of HAKE [26].

Table 6: Rules for the activity “human board an airplane” from the proposed symbolic system and HAKE [26].

C.8 Robustness

We analyze the robustness of the generated symbolic system as follows.

Convergence. The symbol-rule loop should find a symbolic sub-system that "converges". In other words, after a certain stopping criterion, a new round will bring few or even no new symbols to the sub-system. In practice, the stopping criterion is: At most 15 symbols are used for rule extension to avoid semantic redundancy. After that, new symbols are not used for rule extension, leading to a stop of the loop. With the stopping criterion, the symbol-rule loop satisfies convergence. Take Tab.1 as an example: in rounds 1-5, the newly added symbols count is 5, 5, 3, 3, 1, which shows a convergence trend. Fig.5(a) in the main text shows a similar convergence trend. More generally, for the randomly sampled 50 activities, a new round brings an average of 1.9 symbols to the sub-system, verifying the convergence.

Sensitivity to initial conditions. The symbol-rule loop should provide a reliable and stable symbolic sub-system over a range of initial conditions. The sensitivity to initial conditions mainly comes from the asymmetry of rule generation: with 4 as an initial symbol, a rule connecting 4&10&6 is generated, while the rule sometimes cannot be generated with 10 as an initial symbol. However, we find such sensitivity an infrequent case with multiple rules sampling. To verify this, we randomly sample 15 different initial symbol sets to generate the sub-system and then measure the average pairwise graph similarity. The average similarity on 10 randomly sampled activities is 0.91, verifying the low sensitivity to initial conditions.

Sensitivity to different prompts. Experiment results are sensitive to prompts with major differences. Using the older version prompt during the trial-and-error process brings difficulty to correct and automated symbol generation. Experiment results are less sensitive to prompts with minor differences, *i.e.*, slightly paraphrasing the prompts. We conducted a brief experiment: We get another 2 paraphrased symbol init prompts and another 2 paraphrased rule extension prompts. We use these $3 * 3 = 9$ prompts to generate 9 sub-systems and measure the average pairwise graph similarity. The average similarity (range: [-1,1]) on 10 randomly sampled activities is 0.83, verifying the relatively low sensitivity to different prompts.

D More Details of Visual Reasoning

D.1 Visual Symbol Extractor

The visual symbol extractor is based on a VLM BLIP2 [24] with its language model used as a scoring function [1]. A language model represents a distribution over potential completions $p(w_k|w_{<k})$, where w_k is a word that appears at a k -th position in a text. While typical generation applications sample from this distribution, we can also use the model to score a candidate completion selected from a set of options [1]. With a symbol converted into a sentence, *e.g.*, “The person’s hip is seated in a boat. Yes/No?”, the language model outputs the probabilities of constrained responses “Yes” “No” as $p_{y,i}^{(j)}, p_{n,i}^{(j)}$. Then the probability $p_i^{(j)}$ of the symbol can be obtained via normalizing the Yes/No answer with softmax function as:

$$p_i^{(j)} = \frac{e^{p_{y,i}^{(j)}}}{e^{p_{y,i}^{(j)}} + e^{p_{n,i}^{(j)}}}. \quad (4)$$

D.2 Visual Symbol Checker

To check symbols, one symbol $m_i^{(j)}$ is paraphrased [6] into 5 variants $\{m_{i,k}^{(j)}\}_{k=1}^5$. The predictions of variants should be similar due to semantic consistency. Thus, the standard deviation $std_i^{(j)}$ of the predictions $\{p_{i,k}^{(j)}\}_{k=1}^5$ is calculated. In practice, the symbols $m_i^{(j)}$ with $std_i^{(j)} \geq 0.05$ are regarded as uncertain symbols and filtered out. The proportion of filtered symbols is around 5%.

D.3 Dataset and Metric

We conduct experiments on image-level activity understanding benchmarks with diverse tasks.

HICO [5] is a Human-Object Interaction (HOI) recognition benchmark, with 38,116 / 9,658 images in the train/test set. It defines 600 HOIs composed of 117 verbs and 80 COCO objects [30].

Stanford40 [44] is an activity recognition dataset, with 9,532 images for 40 actions. Its train/test set contains 4,000/5,532 images. We omit its bounding box annotations and focus on the image-level recognition task.

HAKE [28, 27] provides 118K+ images, which include 285K human instances, 250K interacted objects, and 724K HOI pairs with human body part states (PaSta) [28, 32]. To utilize the abundant activity samples, we follow the setting in [25] to split HAKE [28], with 22,156 images in the test set. Differently, we design different tasks to facilitate activity reasoning.

HAKE [28, 27]-**Verb** is a verb recognition benchmark that defines 156 verbs related to human activity. To remove ambiguity, the verb prediction is conditioned upon ground-truth object labels, *i.e.*, excluding verbs contradictory to known objects.

HAKE [28, 27]-**PaSta** is a multi-choice QA benchmark to predict PaSta with the ongoing HOIs known as conditions, dealing with finer-grained human activity. To maintain the sample balance of PaSta, we select a subset of 1,438 images from the original one [25] and match a QA pair for each image.

For HICO [5] and HAKE [28, 27]-Verb, we use mAP for multi-label classification. For Stanford40 [44], we use mAP following the original setting. For HAKE [28]-PaSta, we use top-1 accuracy for multi-choice QA.

For HICO [5], HAKE [28]-Verb and Stanford40 [44], symbols and rules are generated in the summarized pipeline in Sec. 3.2.3 in the main text and Sec. C.2 in supplementary.

D.4 Results and Analysis

We further analyze the visual reasoning results in Tab. 2 in the main text.

More baselines. We omit some HICO [5] baselines in the main text because of space limitations. We provide them here in Tab. 7.

| Method | mAP | |
|----------------------------|--------------|--------------|
| | fine-tuned | zero-shot |
| R*CNN [17] | 28.50 | - |
| Girdhar <i>et al.</i> [16] | 34.60 | - |
| Mallya <i>et al.</i> [34] | 36.10 | - |
| Pairwise [10] | 39.90 | - |
| RelViT [33] | 40.10 | - |
| CLIP [37] | 67.12 | 37.08 |
| CLIP [37]+Reason | 69.73 | 43.21 |
| BLIP2 [24] | - | 50.61 |
| BLIP2 [24]+Reason | - | 53.15 |

Table 7: Visual reasoning results on HICO [5].

| Symbol probability | I | II | Symbol probability | I | II |
|---|------|------|---|------|------|
| m_1 : hold a boarding pass | 0.31 | 0.09 | m_{10} : luggage is loaded onto the plane | 0.73 | 0.77 |
| m_2 : place luggage in overhead compartment | 0.86 | 0.76 | m_{11} : reach for the airplane door handle | 0.22 | 0.91 |
| m_3 : adjust seatbelt | 0.47 | 0.97 | m_{12} : stand in line with carry-on luggage | 0.11 | 0.04 |
| m_4 : wave goodbye to loved ones | 0.22 | 0.09 | m_{13} : hold the carry-on luggage | 0.30 | 0.64 |
| m_5 : grip a luggage handle | 0.78 | 0.52 | m_{14} : open the airplane door | 0.34 | 0.91 |
| m_6 : walk towards the boarding gate | 0.21 | 0.05 | m_{15} : move forward in the line | 0.40 | 0.28 |
| m_7 : luggage visible beside him | 0.89 | 0.34 | m_{16} : move towards the airplane door | 0.10 | 0.72 |
| m_8 : boarding pass is scanned by airport staff | 0.86 | 0.07 | m_{17} : airline staff checking the boarding pass | 0.78 | 0.13 |
| m_9 : stand on the jet bridge | 0.54 | 0.44 | | | |

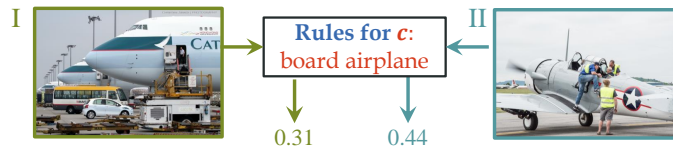


Figure 11: Two failure cases for the activity "human board an airplane". The rules are the same as those in the main paper Tab.1.

Integrating System-1/2-like methods. As a plug-and-play, the reasoning is compatible with existing System-1-like methods. We follow the setting of HAKE [26] to integrate the System-2 reasoning result \mathcal{S}_{sys2} with the prediction \mathcal{S}_{sys1} of System-1-like methods. The final prediction is $\mathcal{S}_{int} = \alpha_1 * \mathcal{S}_{sys1} + \alpha_2 * \mathcal{S}_{sys2}$, where α_1, α_2 is a re-scaling factor to normalize $\mathcal{S}_{sys1}, \mathcal{S}_{sys2}$ and calculated from $\mathcal{S}_{sys1}, \mathcal{S}_{sys2}$.

Performance gap between System-1-like methods. We mainly choose 2 typical System-1-like methods: CLIP [37] and BLIP2 [24]. Comparing the two baselines, we find that with a frozen language model, BLIP2 [24] is more capable of understanding activity semantics and outperforms CLIP [37] in various zero-shot benchmarks. Furthermore, the performance boost from reasoning is more evident on CLIP [37] than on BLIP2 [24]. For example, on HICO [5], visual reasoning improves 6.13 mAP for CLIP [37] while 2.54 mAP for BLIP2 [24]. The performance gap between System-1-like methods can be partly explained by the model ensemble: the visual symbol extractor in reasoning is based on BLIP2 [24], thus applying reasoning to CLIP [37] model brings in more bonus. In ablation studies, we analyze the effects of the model ensemble (Sec. 4.4, the Reasoning section in the main text). We find that trivially combining with baseline results (CLIP [37]+BLIP2 [24]) (44.76 mAP) outperform the baseline CLIP [37] (43.92 mAP), but integrating reasoning is superior (48.95 mAP). It verifies the necessity of System-2 reasoning other than trivially combining predictions from two models.

Performance gap between benchmarks. The performance improvement on HAKE [26]-PaSta is relatively smaller compared with other benchmarks. One possible explanation is the conclusion in HAKE [26]-PaSta is PaSta, which is more with more ambiguity compared with the activity class, *e.g.*, "hold something" vs. "ride a boat". The ambiguity of multi-choice answers hinders reasoning, but it is caused by the inherent ambiguity of the PaSta definition instead of the proposed reasoning method.

However, despite the ambiguity, HAKE [26]-PaSta is still valuable in verifying the effectiveness of reasoning for finer-grained activity understanding tasks.

Failure Cases. We provide two failure cases (false negative) for the activity "human board an airplane" in Fig. 11. In image I, the failure is caused by the prediction error of symbol probabilities. Some symbols are predicted as low probabilities by mistake, *e.g.*, "walk towards the boarding gate". Tiny human bounding boxes possibly cause the symbol prediction error. In image II, the failure emerges because the generated rules do not cover the situation in the image, *i.e.*, errors of the symbolic system. For example, the image contains the symbol "climb up the airplane edge" which is not in the symbolic system.

D.5 Computation Cost

Symbol predictions will increase the computational cost as a trade-off for explainability and generalization. In this paper, we mainly focus on the effectiveness and implementation of our insight and do not preferentially consider efficiency. It can be eased by discovering the hierarchical and reusable nature of the symbols. We show some initial exploration below.

Hierarchical structure. Not all symbols need to be predicted via pruning. Symbols can be organized as a tree with hierarchical prediction. For the Fig.6 example in the main text, $m_1 \dots m_{10}$ can be organized as:

- m_a : Interact with a seller:
 - m_1 : Talk with seller
 - m_3 : Seller hand over orange
 - m_{10} : Give money to seller
- m_b : Interact with the oranges:
 - m_2 : Reach for an orange
- m_c : Interact with a container:
 - m_5 : Place orange in a bag
 - m_6 : Pick orange from a basket
 - m_7 : Hold a bag of oranges
 - m_9 : Seller put the orange in bag
- m_d : Payment Process:
 - m_4 : Stand in front of fruit stand
 - m_8 : Reach for a wallet

The father symbols (*e.g.*, m_a) can be summarized based on the son symbols (*e.g.*, m_1) via simple semantic extraction (*e.g.*, LLM prompt). On the symbol tree, the probability of a son symbol is no higher than its father symbol. When the probability of a father symbol is lower than a threshold (*e.g.*, in image III, m_a probability less than 0.1), its son symbols (m_1 , m_3 , m_{10}) will be assigned the threshold directly without extra computation. Thus, the computational cost is saved via the hierarchical structure of symbols. For example, image III only needs 5 instead of 10 calculations: Interact with a seller(x), Interact with the oranges, Reach for an orange, Interact with a container(x), and Payment Process(x). The computation save will be more evident with the number of symbols scales.

Reusable symbols. The total number of symbols to measure will increase with the number of potential activity classes, but not scale linearly. It is unavoidable to measure probabilities of more than one activity class for activity understanding tasks. This is because activity recognition is a multi-label classification rather than a multi-class classification: A person typically performs multi-action simultaneously, *e.g.*, standing while eating. Thus, the increase in symbol measurement comes from the inherent characteristics of activity tasks. However, the symbols are reused for different activity classes without repetitive computation. For example, "buy orange" and "visit store" shares the symbols: (m_a) Interact with a seller, (m_d) Payment process, (m_1) Talk with the seller, (m_{10}) Give money to the seller, (m_8) Reach for a wallet. It is also illustrated in the main paper Fig.2(a): the red and green activities share some symbols (gray), *e.g.*, second from right, third from left.

Quantitative comparison. We provide a detailed analysis of a small case. There are 38 images known to contain oranges, where verbs (buy/cut/eat/hold/inspect/peel/pick/squeeze/wash) are to be predicted. We report the number of operations average per image on it. Without reasoning, activity classes are predicted directly, and the number of operations varies from images due to different ground-truth object labels which verb prediction conditions upon. The average number of operations is 9. With reasoning, the average number of operations is 71. However, with reusable symbols, the number is reduced to 31, and adding a hierarchical structure further reduces it to 23.



What are person on the right doing?

- a) person on the left is taking person on the right home.
- b) person on the right are on a first date.**
- c) person on the left is conducting a job interview with person on the right.
- d) They are picking something up.

Figure 12: An example QA in VCR dataset.

E Boarder Application

The method could be more general and facilitate real-world applications. We choose activity understanding as a good and important initial test bed because it is a difficult task with complex visual patterns and a compositional nature. The proposed symbolic system can be generalized to various tasks (*e.g.*, classification, visual commonsense) with a similar formulation. Semantic coverage and logical entailment remain two important properties under a more general setting, and we can reason with visual inputs via a similar pipeline. We show two initial experiments below.

Object classification. One example rule for an object (*e.g.*, crocodile) is: long, slightly curved body \wedge four short legs \wedge ... \wedge a long, muscular tail \rightarrow crocodile. We conduct experiments on CIFAR-100 [22] test set with a zero-shot setting. The performance is 77.50% accuracy for CLIP and 78.31% accuracy for CLIP+Reasoning.

Visual commonsense. One example rule for the image and question in Fig. 12 is: person on the right shows affectionate gestures \wedge person on the left engages in conversation \wedge ... \wedge The environment is a restaurant \rightarrow b. We conduct experiments on VCR [47] val set. BLIP2 is adopted as a baseline as it is a VQA-style task. VCR val set has 26534 image-question pairs, where we select a subset of 557 pairs for the test. The selected pairs are highly related to human activities (instead of role, mental, *etc*) and only involve *one* person’s activity. The performance is 46.32% accuracy for BLIP2 and 47.08% accuracy for BLIP2+Reasoning.

We can see that the proposed pipeline can be applied to general visual tasks and facilitate reasoning. In this paper, we focus on method design instead of task generalization. We will analyze more general settings in future work.

References

- [1] Michael Ahn, Anthony Brohan, Noah Brown, Yevgen Chebotar, Omar Cortes, Byron David, Chelsea Finn, Keerthana Gopalakrishnan, Karol Hausman, Alex Herzog, et al. Do as i can, not as i say: Grounding language in robotic affordances. *arXiv preprint arXiv:2204.01691*, 2022.
- [2] Jacob Andreas, Marcus Rohrbach, Trevor Darrell, and Dan Klein. Neural module networks. In *CVPR*, 2016.
- [3] Claude Berge. *Hypergraphs: combinatorics of finite sets*, volume 45. Elsevier, 1984.
- [4] Joao Carreira and Andrew Zisserman. Quo vadis, action recognition? a new model and the kinetics dataset. In *CVPR*, 2017.
- [5] Yu Wei Chao, Zhan Wang, Yugeng He, Jiaxuan Wang, and Jia Deng. Hico: A benchmark for recognizing human-object interactions in images. In *ICCV*, 2015.
- [6] Prithviraj Damodaran. Parrot: Paraphrase generation for nlu., 2021.

- [7] Honghua Dong, Jiayuan Mao, Tian Lin, Chong Wang, Lihong Li, and Denny Zhou. Neural logic machines. *arXiv preprint arXiv:1904.11694*, 2019.
- [8] Yong Du, Wei Wang, and Liang Wang. Hierarchical recurrent neural network for skeleton based action recognition. In *CVPR*, 2015.
- [9] Richard Evans, David Saxton, David Amos, Pushmeet Kohli, and Edward Grefenstette. Can neural networks understand logical entailment? *arXiv preprint arXiv:1802.08535*, 2018.
- [10] Hao Shu Fang, Jinkun Cao, Yu Wing Tai, and Cewu Lu. Pairwise body-part attention for recognizing human-object interactions. In *ECCV*, 2018.
- [11] Hao-Shu Fang, Jiefeng Li, Hongyang Tang, Chao Xu, Haoyi Zhu, Yuliang Xiu, Yong-Lu Li, and Cewu Lu. Alphapose: Whole-body regional multi-person pose estimation and tracking in real-time. *TPAMI*, 2023.
- [12] Christoph Feichtenhofer, Haoqi Fan, Jitendra Malik, and Kaiming He. Slowfast networks for video recognition. In *ICCV*, 2019.
- [13] Daan Fierens, Guy Van den Broeck, Joris Renkens, Dimitar Shterionov, Bernd Gutmann, Ingo Thon, Gerda Janssens, and Luc De Raedt. Inference and learning in probabilistic logic programs using weighted boolean formulas. *Theory and Practice of Logic Programming*, 15(3):358–401, 2015.
- [14] Giorgio Gallo, Giustino Longo, Stefano Pallottino, and Sang Nguyen. Directed hypergraphs and applications. *Discrete applied mathematics*, 42(2-3):177–201, 1993.
- [15] Artur d’Avila Garcez, Marco Gori, Luis C Lamb, Luciano Serafini, Michael Spranger, and Son N Tran. Neural-symbolic computing: An effective methodology for principled integration of machine learning and reasoning. *arXiv preprint arXiv:1905.06088*, 2019.
- [16] Rohit Girdhar and Deva Ramanan. Attentional pooling for action recognition. *NeurIPS*, 2017.
- [17] Georgia Gkioxari, Ross Girshick, and Jitendra Malik. Contextual action recognition with r* cnn. In *ICCV*, 2015.
- [18] Chunhui Gu, Chen Sun, David A Ross, Carl Vondrick, Caroline Pantofaru, Yeqing Li, Sudheendra Vijayanarasimhan, George Toderici, Susanna Ricco, Rahul Sukthankar, et al. Ava: A video dataset of spatio-temporally localized atomic visual actions. In *CVPR*, 2018.
- [19] Saurabh Gupta and Jitendra Malik. Visual semantic role labeling. *arXiv preprint arXiv:1505.04474*, 2015.
- [20] Drew Hudson and Christopher D Manning. Learning by abstraction: The neural state machine. *NeurIPS*, 2019.
- [21] Chao Jia, Yinfei Yang, Ye Xia, Yi-Ting Chen, Zarana Parekh, Hieu Pham, Quoc Le, Yun-Hsuan Sung, Zhen Li, and Tom Duerig. Scaling up visual and vision-language representation learning with noisy text supervision. In *ICML*, 2021.
- [22] Alex Krizhevsky, Geoffrey Hinton, et al. Learning multiple layers of features from tiny images. 2009.
- [23] Sumith Kulal, Jiayuan Mao, Alex Aiken, and Jiajun Wu. Hierarchical motion understanding via motion programs. In *CVPR*, 2021.
- [24] Junnan Li, Dongxu Li, Silvio Savarese, and Steven Hoi. Blip-2: Bootstrapping language-image pre-training with frozen image encoders and large language models. *arXiv preprint arXiv:2301.12597*, 2023.
- [25] Yong-Lu Li, Xinpeng Liu, Xiaoqian Wu, Xijie Huang, Liang Xu, and Cewu Lu. Transferable interactiveness knowledge for human-object interaction detection. *TPAMI*, 2022.
- [26] Yong-Lu Li, Xinpeng Liu, Xiaoqian Wu, Yizhuo Li, Zuoyu Qiu, Liang Xu, Yue Xu, Hao-Shu Fang, and Cewu Lu. Hake: a knowledge engine foundation for human activity understanding. *TPAMI*, 2022.
- [27] Yong-Lu Li, Liang Xu, Xinpeng Liu, Xijie Huang, Yue Xu, Mingyang Chen, Ze Ma, Shiyi Wang, Hao-Shu Fang, and Cewu Lu. Hake: Human activity knowledge engine. *arXiv preprint arXiv:1904.06539*, 2019.
- [28] Yong-Lu Li, Liang Xu, Xinpeng Liu, Xijie Huang, Yue Xu, Shiyi Wang, Hao-Shu Fang, Ze Ma, Mingyang Chen, and Cewu Lu. Pastanet: Toward human activity knowledge engine. In *CVPR*, 2020.
- [29] Ji Lin, Chuang Gan, and Song Han. Tsm: Temporal shift module for efficient video understanding. In *ICCV*, 2019.

- [30] Tsung Yi Lin, Michael Maire, Serge Belongie, James Hays, Pietro Perona, Deva Ramanan, Piotr Dollár, and C. Lawrence Zitnick. Microsoft coco: Common objects in context. In *ECCV*, 2014.
- [31] Yunchao Liu and Zheng Wu. Learning to describe scenes with programs. In *ICLR*, 2019.
- [32] Cewu Lu, Hao Su, Yonglu Li, Yongyi Lu, Li Yi, Chi-Keung Tang, and Leonidas J Guibas. Beyond holistic object recognition: Enriching image understanding with part states. In *CVPR*, 2018.
- [33] Xiaojian Ma, Weili Nie, Zhiding Yu, Huaizu Jiang, Chaowei Xiao, Yuke Zhu, Song-Chun Zhu, and Anima Anandkumar. Relvit: Concept-guided vision transformer for visual relational reasoning. *arXiv preprint arXiv:2204.11167*, 2022.
- [34] Arun Mallya and Svetlana Lazebnik. Learning models for actions and person-object interactions with transfer to question answering. In *ECCV*, 2016.
- [35] Kenneth Marino, Xinlei Chen, Devi Parikh, Abhinav Gupta, and Marcus Rohrbach. Krisp: Integrating implicit and symbolic knowledge for open-domain knowledge-based vqa. In *CVPR*, 2021.
- [36] Maxwell Nye, Michael Tessler, Josh Tenenbaum, and Brenden M Lake. Improving coherence and consistency in neural sequence models with dual-system, neuro-symbolic reasoning. *NeurIPS*, 2021.
- [37] Alec Radford, Jong Wook Kim, Chris Hallacy, Aditya Ramesh, Gabriel Goh, Sandhini Agarwal, Girish Sastry, Amanda Askell, Pamela Mishkin, Jack Clark, et al. Learning transferable visual models from natural language supervision. In *ICML*, 2021.
- [38] Luc De Raedt, Kristian Kersting, Sriraam Natarajan, and David Poole. Statistical relational artificial intelligence: Logic, probability, and computation. *Synthesis lectures on artificial intelligence and machine learning*, 10(2):1–189, 2016.
- [39] Shaoqing Ren, Kaiming He, Ross Girshick, and Jian Sun. Faster r-cnn: Towards real-time object detection with region proposal networks. In *NeurIPS*, 2015.
- [40] Botian Shi, Lei Ji, Pan Lu, Zhendong Niu, and Nan Duan. Knowledge aware semantic concept expansion for image-text matching. In *IJCAI*, volume 1, page 2, 2019.
- [41] Amanpreet Singh, Ronghang Hu, Vedanuj Goswami, Guillaume Couairon, Wojciech Galuba, Marcus Rohrbach, and Douwe Kiela. Flava: A foundational language and vision alignment model. In *CVPR*, 2022.
- [42] Raviteja Vemulapalli, Felipe Arrate, and Rama Chellappa. Human action recognition by representing 3d skeletons as points in a lie group. In *CVPR*, 2014.
- [43] Yue Xu, Yong-Lu Li, Jiefeng Li, and Cewu Lu. Constructing balance from imbalance for long-tailed image recognition. In *ECCV*, 2022.
- [44] Bangpeng Yao, Xiaoye Jiang, Aditya Khosla, Andy Lai Lin, Leonidas Guibas, and Li Fei-Fei. Human action recognition by learning bases of action attributes and parts. In *ICCV*, 2011.
- [45] Kexin Yi, Jiajun Wu, Chuang Gan, Antonio Torralba, Pushmeet Kohli, and Josh Tenenbaum. Neural-symbolic vqa: Disentangling reasoning from vision and language understanding. *NeurIPS*, 2018.
- [46] L Zadeh. Fuzzy sets. *Inform Control*, 8:338–353, 1965.
- [47] Rowan Zellers, Yonatan Bisk, Ali Farhadi, and Yejin Choi. From recognition to cognition: Visual commonsense reasoning. In *CVPR*, 2019.
- [48] Jingyi Zhang, Jiaxing Huang, Sheng Jin, and Shijian Lu. Vision-language models for vision tasks: A survey. *arXiv preprint arXiv:2304.00685*, 2023.